J. Fluid Mech. (1995), *vol.* 305, *pp.* 239–261

The effects of temperature-dependent viscosity on flow in a cooled channel with application to basaltic fissure eruptions

By JONATHAN J. WYLIE AND JOHN R. LISTER

Institute of Theoretical Geophysics, Department of Applied Mathematics and Theoretical Physics, Silver Street, Cambridge CB3 9EW, UK.

(Received 1 May 1995 and in revised form 10 August 1995)

A theoretical description is given of pressure-driven viscous flow of an initially hot fluid through a planar channel with cold walls. The viscosity of the fluid is assumed to be a function only of its temperature. If the viscosity variations caused by the cooling of the fluid are sufficiently large then the relationship between the pressure drop and the flow rate is non-monotonic and there can be more than one steady flow for a given pressure drop. The linear stability of steady flows to two-dimensional and three-dimensional disturbances is calculated. The region of instability to two-dimensional disturbances corresponds exactly to those flows in which an increase in flow rate leads to a decrease in pressure drop. At higher viscosity contrasts some flows are most unstable to three-dimensional (fingering) instabilities analogous, but not identical, to Saffman–Taylor fingering. A cross-channel-averaged model is derived and used to investigate the finite-amplitude evolution.

1. Introduction

The viscosity of most fluids increases on cooling. Large changes in the viscosity of fluids occur in industrial processes such as injection moulding and glass manufacture and in geological situations such as volcanic eruptions and lava flows. When hot molten rock flows into a much cooler environment, the resultant cooling causes polymerization of silicates within the magma and leads to a dramatic increase in the viscosity. Rheological variations in the flow, from a hot interior to a cooled exterior, or from source to distal regions, lead to a number of important phenomena. These range from local instabilities such as the formation of pahoehoe toes at the front of lava flows where hot fluid pushes through a chilled viscous skin, to global effects on the flow such as channelization by the formation of solidified levees at the sides of the flow or 'buckling' of the flows (which would be catastrophic in the manufacture of glass). The rheological variation will also control the rate at which lava flows propagate and the total distance that they flow before solidification. This is clearly of interest to populations living in the vicinity of regions where volcanic activity occurs.

A number of non-explosive basaltic eruptions have been observed in Hawaii (Richter *et al.* 1970) and Iceland (Björnsson *et al.* 1979). Hot magma is stored in large chambers just a few kilometres below the surface of the Earth. Typically the eruptions begin with the rapid opening of fissures whose linear extent is much greater than their width. The magma flows from the chamber through the fissures toward the surface driven by the high pressures typical in magma chambers. On reaching the

surface the flow can fountain up to heights of tens of metres forming a 'curtain of fire'. After a few hours the flow rate is observed to decrease. In some cases the flow rate is also observed to vary along the length of the fissure and after a further few hours solidification transforms the fissure into a number of small isolated surface vents. It is thought that the evolution and focusing of the flow is due to the interaction of the flow and the rheological variation in the magma on cooling (Bruce & Huppert 1990).

Motivated by these observations, we analyse a simple model that provides a theoretical description of channel flows in which a large increase occurs in the viscosity. We model a fissure by a rectangular conduit and model the cooling effect of the surrounding rock by prescribing a constant temperature on the walls of the conduit. The flow is considered to be driven by a constant pressure drop over the length of the conduit, which is a more appropriate boundary condition than that of constant mass flux for geological situations and for all but the very early stages of injection moulding. We suppose that the fluid is Newtonian, but with a viscosity that is a given function of temperature.

Despite the relevance of problems involving large viscosity variations to industrial and geological processes, there have been surprisingly few previous studies. Ockendon & Ockendon (1977) considered two-dimensional steady flows driven by a constant mass flux through a rectangular conduit whose walls are maintained at a constant temperature. Effects of mechanical inertia were neglected and the lubrication approximation made to the momentum and temperature equations. Under these assumptions, Ockendon & Ockendon determined the asymptotic structure of the velocity and temperature fields for the particular cases of algebraic and exponential relationships between viscosity and temperature at asymptotically large viscosity variation.

Richardson (1986) extended the work of Ockendon & Ockendon (1977) to include some of the effects of solidification. He employed a viscosity model which depended exponentially on the temperature and as a power law of the local shear rate, and also examined the case of asymptotically large viscosity contrasts for steady two-dimensional flows. By considering only high flow rates, he showed that an increase in the flow rate can lead to a decrease in the pressure drop, but did not investigate this phenomenon in detail.

Whitehead & Helfrich (1991) considered a conduit fed by an elastic chamber and a viscosity which depends linearly on the temperature. By considering a much simplified one-dimensional model in which the cross-flow structure is represented heuristically by an average, they produced a plausible description of the system for all flow rates. They predicted that for sufficiently large viscosity contrasts certain pressure drops can be attained by three different steady flow rates. They introduced the effects of mechanical inertia rather than thermal inertia, which is inappropriate for the large Prandtl numbers characteristic of geological flows, in order to consider the stability of the steady flows to variations in the along-fissure direction. However, the results of the stability calculation were inconclusive since the largest growth rates occurred for large wavenumbers. They recognized that an improved model incorporating lateral flow in the conduit would be necessary to determine the stability characteristics of the basic steady flow to along-conduit variations.

Bruce & Huppert (1990) considered the effects of solidification and melting in a conduit with flow driven by a constant pressure drop. The fluid in their analysis was assumed to be of constant viscosity, but the width of the channel varied due to the solidification and melting thus varying the flow resistance in the conduit. Their analysis showed that if the initial width was greater than some critical value then the walls of the conduit would eventually melt away but if the initial width was less than

the critical value then solidification would eventually block the conduit. Owing to the thermal boundary conditions imposed by embedding the conduit in an infinite solid, the calculation was necessarily time-dependent, which precluded a formal stability calculation around a steady basic state. However, by using simple physical reasoning they proposed a mechanism that might lead to instability and along-fissure flow localization.

While these studies have suggested the possibility of instabilities and interesting nonlinear dynamics, the suggestions have previously been unconfirmed by quantitative analysis. The objective of the present work is to calculate the steady states for flow in a rectangular conduit with temperature-dependent viscosity and to subject these states to a formal stability analysis. (In the preceding paper in this volume Helfrich (1995) presents an approximate analysis based on cross-channel averages of this problem.) In §2 the equations governing heat and mass transport within a rectangular conduit are derived under geologically relevant assumptions. The system can be described by two dimensionless parameters. The first represents the magnitude of the variation in viscosity and the second is a measure of the speed of the flow through the conduit, which can also be thought of as being a measure of the pressure drop. In §3 a particularly efficient numerical method is formulated to obtain steady two-dimensional solutions for a range of flow rates. It is shown that for sufficiently large viscosity variations the relationship between pressure drop and flow rate becomes non-monotonic so that there can be three different steady states for a given pressure drop. A physical explanation for this phenomenon is provided, along with a discussion of the effect of the form of the viscosity–temperature relationship.

The linear stability of the two-dimensional steady states to three-dimensional disturbances is considered in §4. With conventional techniques this stability problem would represent a computationally expensive task. However, an idea similar to that used to solve for the basic state can be used to derive another efficient numerical method for the stability problem. The results show that flows which are stable to two-dimensional disturbances can become destabilized by three-dimensional perturbations. A physical explanation which draws an analogy with the Saffman–Taylor (1958) instability is provided.

The instability of some two-dimensional states raises the question of what they evolve to. This question motivates §§5 and 6 in which we examine the possibility of three-dimensional (flow-focused) steady states. Section 5 contains the proof of a surprising result which demonstrates a close correspondence between the structure of three-dimensional and two-dimensional steady states. In §6 we make use of this result to produce a numerical method which is then utilized to seek three-dimensional steady states. The results are discussed and compared with previous results in §7. The applications to geology are also explored.

2. Problem formulation

Consider a fluid of constant density ρ and thermal diffusivity κ flowing through a rectilinear channel of width $2d$, length L and infinite lateral extent (figure 1). We define coordinates in which $z = 0$ and $z = L$ correspond to the fluid entrance and exit of the channel respectively, the walls of the channel are located at $y = \pm d$ and the x-direction is perpendicular to the y- and z-directions. The origin of the x-coordinate is arbitrary due to the infinite lateral extent of the channel in that direction. We introduce, for convenience, the terminology 'along-channel' for the z-direction, 'cross-channel' for the y-direction and 'transverse' for the x-direction.

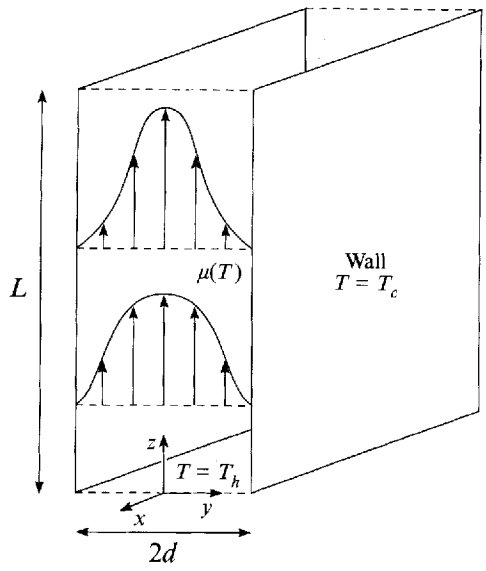

FIGURE 1. Definition sketch. A fluid of constant density and thermal diffusivity is driven by a constant pressure drop through a rectilinear channel of length L, width $2d$ and infinite extent in the x-direction. The temperature of the input fluid is T_h and that of the channel walls is maintained at T_c; the viscosity μ of the fluid varies with its temperature.

Let the channel walls be maintained at a constant temperature T_c and the input temperature of the fluid at temperature T_h, where $T_h > T_c$. Let the flow be driven by a constant pressure drop ΔP over the length of the channel. We suppose that the variation of the fluid viscosity with temperature is given by $\mu(T)$ and take the viscosity at the input temperature, $\mu_h = \mu(T_h)$, as the reference value in dimensional scalings.

Parameter values for basaltic eruptions vary widely, but typical order-of-magnitude estimates are $d \sim 0.3\,\mathrm{m}$, $L \sim 10\,\mathrm{km}$, $\rho \sim 3000\,\mathrm{kg\,m^{-3}}$, $\kappa \sim 10^{-6}\,\mathrm{m^2 s^{-1}}$, $T_h - T_c \sim 100\,\mathrm{K}$, $\Delta P/L \sim 10^3\,\mathrm{Pa\,m^{-1}}$, $\mu_h \sim 100\,\mathrm{Pa\,s}$ and thermal conductivity $k \sim 3\,\mathrm{W\,K^{-1}m^{-1}}$ (e.g. Bruce & Huppert 1990). These estimates suggest that

$$Re \equiv \frac{\rho \Delta P d^3}{\mu_h^2 L} \sim 10 \tag{2.1}$$

is sufficiently small that the flow is laminar and that

$$Re\,\frac{d}{L} \sim 3 \times 10^{-4} \ll 1, \tag{2.2a}$$

$$\frac{d}{L} \sim 3 \times 10^{-5} \ll 1, \tag{2.2b}$$

$$Pe \equiv \frac{\Delta P d^3}{\kappa \mu_h L} \sim 3 \times 10^5 \gg 1, \tag{2.2c}$$

and

$$Pr \equiv \frac{\mu_h}{\rho \kappa} \sim 3 \times 10^4 \gg 1. \tag{2.2d}$$

The effects of mechanical inertia can be neglected because of (2.2a). Along-channel and transverse diffusion of momentum and heat can be neglected owing to (2.2b). Along-stream diffusion of heat is negligible compared to advection of heat owing to

(2.2*c*). The thermal entry length is much longer than the mechanical entry length because of (2.2*d*) and so Poiseuille flow at the input can be assumed. As in previous studies (e.g. Bruce & Huppert 1990; Whitehead & Helfrich 1991), though the Brinkman number is not particularly small ($\Delta P^2 d^4/\mu_h L^2 k(T_h - T_c) \sim 0.3$), we also neglect the effects of viscous heating for simplicity. In geological applications these effects will be offset by cooling due to adiabatic decompression, which we also neglect.

We define dimensionless variables by

$$\hat{T} \equiv \frac{T - T_c}{T_h - T_c}, \qquad \hat{p} \equiv \frac{d^4}{\mu_h \kappa L^2} p, \qquad \hat{\mu}(\hat{T}) \equiv \frac{\mu(T)}{\mu_h}, \tag{2.3a,b,c}$$

$$\hat{t} \equiv \frac{\kappa}{d^2} t, \qquad \hat{y} \equiv \frac{y}{d}, \qquad (\hat{x}, \hat{z}) \equiv \frac{1}{L}(x, z), \tag{2.3d,e,f}$$

$$\hat{v} \equiv v \frac{d}{\kappa}, \qquad (\hat{u}, \hat{w}) \equiv \frac{d^2}{\kappa L}(u, w), \tag{2.3g,h}$$

where (u, v, w) denotes the fluid velocity. It proves convenient in later sections to denote the velocity and gradient in the plane of the channel by $\boldsymbol{u} \equiv (u, 0, w)$ and $\nabla \equiv (\partial_x, 0, \partial_z)$ respectively.

As a result of the conditions (2.1) and (2.2), and using the non-dimensionalization defined by (2.3), conservation of heat is represented by

$$\frac{\partial T}{\partial t} + \boldsymbol{u} \cdot \nabla T + v T_y = T_{yy}\,, \tag{2.4}$$

where here and in the rest of the paper we have dropped the hats on the dimensionless variables. The momentum equation reduces to the lubrication approximation

$$(\mu(T)\boldsymbol{u}_y)_y = \nabla p, \tag{2.5a}$$

$$0 = p_y. \tag{2.5b}$$

Conservation of mass is given by

$$\nabla \cdot \boldsymbol{u} + v_y = 0. \tag{2.6}$$

The appropriate boundary conditions are those of fixed temperature and zero velocity at the channel walls, fixed temperature and pressure at the entrance, and a downstream condition of fixed pressure at the channel exit. In a time-dependent problem these conditions must be supplemented by suitable initial conditions. Using symmetry of the flow around $y = 0$, these dimensionless boundary conditions can be written

$$T = 0 \quad \text{and} \quad u = v = w = 0 \quad \text{on} \quad y = 1, \tag{2.7a}$$

$$T_y = u_y = v = w_y = 0 \quad \text{on} \quad y = 0, \tag{2.7b}$$

$$T = 1 \quad \text{and} \quad p = 0 \quad \text{on} \quad z = 0, \tag{2.7c}$$

$$p = -\Pi \quad \text{on} \quad z = 1, \tag{2.7d}$$

where

$$\Pi \equiv \frac{\Delta P d^4}{\kappa \mu_h L^2}. \tag{2.8}$$

The parameter Π can be thought of as a dimensionless pressure drop. Alternatively $\Pi^{1/2}$ can be thought of either as the ratio of the thermal relaxation length to the length of the channel, or as the ratio of along-channel advection of heat to cross-channel diffusion of heat. Thus $\Pi \gg 1$ corresponds to the limit in which the pressure difference drives the fluid through the channel so rapidly that cooling only occurs in

thin boundary layers near the walls and $\Pi \ll 1$ corresponds to the limit in which the fluid is cooled very soon after entering the channel and leaves the channel at very close to the temperature of the wall.

In general, the relationship between viscosity and temperature will depend on the fluid in question and must be determined empirically. The viscosities of magmas vary by roughly an order-of-magnitude over 100 K with an even greater rate of variation over temperatures close to the liquidus (Ryan & Blevins 1987). The form of the variation varies from magma to magma, according to composition, volatile content, etc., and would require a number of parameters to describe. For simplicity, we consider the one-parameter functional form

$$\mu(T) = \beta^{1-T}, \tag{2.9a}$$

which gives good experimental agreement, often over quite large temperature variations, for a wide range of fluids including lubricating oils, glycerol and most viscous syrups. We also consider the simple relationship in which viscosity is a step function of temperature,

$$\mu = \begin{cases} 1 \text{ if } T > \theta \\ \beta \text{ if } T < \theta, \end{cases} \tag{2.9b}$$

where θ is a constant, which also captures the basic property that flow resistance should increase with decreasing temperature and has the obvious advantage of easing the analysis. We will perform the theoretical analysis for a general relationship between viscosity and temperature and illustrate the results by using the two examples of (2.9). It is not expected that the qualitative behaviour will depend on the detailed form of this relationship. Irrespective of the form of $\mu(T)$, the dimensionless parameter

$$\beta \equiv \frac{\mu(T_c)}{\mu(T_h)}, \tag{2.10}$$

is implicitly introduced, which we will use to describe the strength of the variation in the viscosity.

3. Steady two-dimensional flows

Steady two-dimensional solutions clearly exist for the case of an isoviscous fluid ($\beta = 1$) and physical considerations suggest that they will persist for $\beta > 1$. Hence we consider (2.4)–(2.7) with $\partial_t \equiv \partial_x \equiv u \equiv 0$.

Given the velocity, the equations for the temperature are parabolic in the direction of flow; whereas, given the temperature, the equations for the velocity are elliptic in the sense that the pressure must satisfy boundary conditions at both the channel entrance and exit, thus making solution a non-trivial matter. However, we observe that the flow rate in a steady two-dimensional solution is constant along the channel so that, given an input flow rate, the remnant system (2.4)–(2.7c) is parabolic and can simply be integrated downstream. With this in mind, we consider (2.4)–(2.7c), and replace the downstream boundary condition $p = -\Pi$ at $z = 1$ by the condition $p_z = -1$ at $z = 0$, which is equivalent to specifying a particular input flow rate. We denote the variables in this system by tildes and integrate forward in $\tilde{z}$ to yield a pressure distribution $\tilde{p}(\tilde{z})$.

We now have a solution which satisfies all the boundary conditions except the downstream pressure condition. It is easy to see that increasing the input flow rate is equivalent to decreasing the length of the channel and so we consider the following

rescaling. For any given value of $\tilde{z}$, say $\tilde{z}_1$, adoption of the rescaling

$$p = \tilde{p}/\tilde{z}_1^2, \qquad z = \tilde{z}/\tilde{z}_1, \qquad w = \tilde{w}/\tilde{z}_1, \tag{3.1}$$

with the other variables left unscaled, yields solutions p, w, v and T which satisfy the two-dimensional steady-state equations with downstream boundary condition $p = \tilde{p}(\tilde{z}_1)/\tilde{z}_1^2$ at $z = 1$, which is equivalent to setting $\Pi = -\tilde{p}(\tilde{z}_1)/\tilde{z}_1^2$. The dimensionless flow rate, Q, is given by

$$Q \equiv 2\int_0^1 w \, \mathrm{d}y = \frac{-2p_z(0)}{3} = \frac{2}{3\tilde{z}_1}. \tag{3.2}$$

It follows that the elliptic system (prescribed pressure drop) can be solved for an array of pressure drops by solving the parabolic system (prescribed flux) just once and then making a number of trivial rescalings. For the purposes of numerical solution this transformation lessens the workload considerably.

3.1. *Numerical scheme*

In order to solve the prescribed-flux problem numerically, we introduce a stream function ψ, defined by $w \equiv \psi_y$, $v \equiv -\psi_z$ and $\psi = 0$ at $y = 0$. By integrating (2.5a) across the channel and applying symmetry at the centreline, we obtain

$$\mu(T)\psi_{yy} = yp_z \tag{3.3a}$$

with boundary conditions

$$\psi = \tfrac{1}{3} \text{ and } \psi_y = 0 \text{ at } y = 1 \tag{3.3b}$$

and

$$\psi = 0 \text{ at } y = 0. \tag{3.3c}$$

Given $\mu(T)$ at a particular value of z, we can find the velocity profile by using the second-order midpoint rule to integrate (3.3*a*) from $y = 1$ subject to (3.3*b*) and then by using (3.3*c*) to determine p_z. Given the velocity field, we can solve the temperature equation (2.4) by using a finite-difference scheme that is second order in both y and z. These solutions, for the velocity given $\mu(T)$ and for T given the velocity, form the basis of an iterative scheme for making a step in the along-channel direction; we use the velocity profile at the previous upstream location as an initial guess for the velocity profile at the current location, solve (2.4) for the temperature distribution at the current location and then (3.3) for a better estimate of the velocity profile. A few iterations of (2.4) and (3.3) produces a convergent solution and then the next along-channel step is made.

For the case in which the viscosity is the step function of temperature defined by (2.9*b*) a slightly different approach is adopted. The system (2.4)–(2.7) can be written as a nonlinear free-boundary problem (or a moving-boundary problem when the system is transformed to its parabolic form) in which the free boundary is given by the isotherm $T = \theta$. The appropriate conditions to be applied across the isotherm are those of continuous temperature, temperature gradient, velocity and stress. We denote the position of the isotherm $T = \theta$ by $Y(z)$ and map the regions $0 < y < Y(z)$ and $Y(z) < y < 1$ onto fixed domains by appropriate boundary-fixing transformations. Given the position of the isotherm $Y(z)$, the velocity profile and pressure gradient can be found analytically (see Appendix A) and the temperature equation (2.4) solved numerically in each domain subject to $T = \theta$ at $y = Y(z)$. The position of $Y(z)$

is determined by the condition that the solutions for T in the two domains have the same gradient at $y = Y(z)$. Hence by treating the difference in the temperature gradients as a function of Y, we can use Brent's method of root finding (Press *et al.* 1992) to ensure that this difference is zero at each along-channel step.

Since hot fluid instantaneously comes into contact with the cold wall at the input, the solution is singular there. Consideration of the local behaviour shows that a thermal boundary layer is produced next to the wall, which initially is unaffected by the finite width of the channel. This absence of a lengthscale gives rise to a similarity solution, which is given by

$$\psi = \tfrac{1}{3} + z^{2/3} f\left(\frac{1-y}{z^{1/3}}\right), \qquad T = g\left(\frac{1-y}{z^{1/3}}\right), \tag{3.4}$$

where

$$\mu(g)\frac{\mathrm{d}^2 f}{d\eta^2} = -1, \qquad \frac{\mathrm{d}^2 g}{\mathrm{d}\eta^2} = \frac{2}{3} f \frac{\mathrm{d}g}{\mathrm{d}\eta} \tag{3.5a,b}$$

from (3.3*a*) and (2.4) respectively. The boundary conditions are

$$f(0) = \frac{\mathrm{d}f}{\mathrm{d}\eta}(0) = g(0) = 0 \text{ and } g(\infty) = 1. \tag{3.5c}$$

This can readily be solved numerically by use of a shooting technique. The solution is shown in figure 2 for the exponential viscosity model and is given in Appendix A for the step-function model. The similarity solution can be used as an 'initial' condition for the numerical solution of (2.4)–(2.7), thus bypassing the problem of the singular input conditions. The self-similar nature of the solution near the input requires the use of a variable step length and a grid that takes into account the fact that the majority of the temperature adjustment initially occurs close to the wall. The similarity solution also provides a valuable check on the accuracy of the numerical method.

3.2. *Results*

The results for both the exponential and the step-function viscosity models show that for sufficiently small β the flow rate is uniquely determined by the pressure drop. However, when β exceeds a critical value, β_c, which depends on the viscosity model, the relationship between pressure drop and flow rate becomes non-monotonic so that there are values of the pressure drop for which the flow rate is no longer uniquely determined (figure 3). In these cases there are three possible flow rates for a given pressure drop. The boundary in (Π, β)-space between the region where there is a unique solution and the region where there are three solutions for a given pressure drop forms a cusp (figure 4). When $\beta > \beta_c$ and the curve relating pressure drop and flow rate is non-monotonic we refer to the portion of the curve between the two local extrema as the central branch, the part of the curve to the right of the local minimum as the fast branch and the part of the curve to the left of the local maximum as the slow branch. The central branch has the property that the pressure drop decreases with increasing flow rate.

The existence of multiple solutions for a given pressure drop can be understood physically by recalling that the pressure drop over the channel length is due to the integrated product of the viscosity and the shear rate and realizing that an increase in flow rate gives rise to two competing effects. Firstly, there is the effect experienced by isoviscous fluids, that increasing the flow rate increases the shear rate, which tends

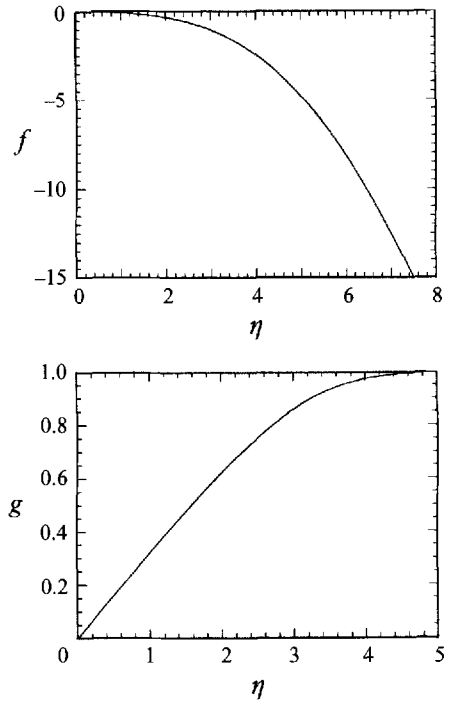

FIGURE 2. The near-entry similarity solutions for the stream function and temperature distribution, as given by (3.4) and (3.5) as functions f and g of the similarity variable $\eta = (1 - y)/x^{1/3}$. The exponential viscosity model (2.9*a*) is used with viscosity ratio $\beta = 10$.

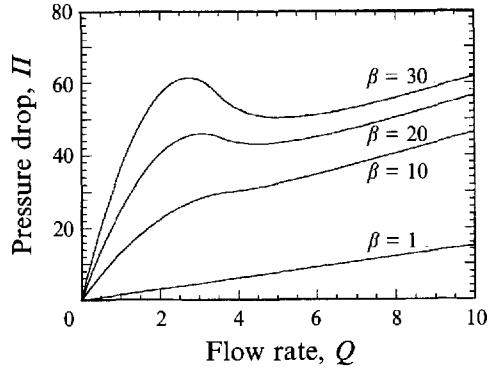

FIGURE 3. The relationship between pressure drop and flow rate for various values of the viscosity ratio β. The viscosity model used is the step-function (2.9*b*) with the step at $\theta = 1/2$.

to give rise to a larger viscous pressure drop. Secondly, an increase in the flow rate decreases the time available for cooling, and thus increases the exit temperature of the fluid and decreases the average viscosity in the channel, which tends to decrease the viscous pressure drop. If the second effect becomes greater than the first then triple-valued solutions will result.

From the above argument it is clear that the functional form of the relationship between viscosity and temperature can have a significant effect on the value of the critical viscosity ratio β_c. As we have seen, a triple-valued solution occurs when the

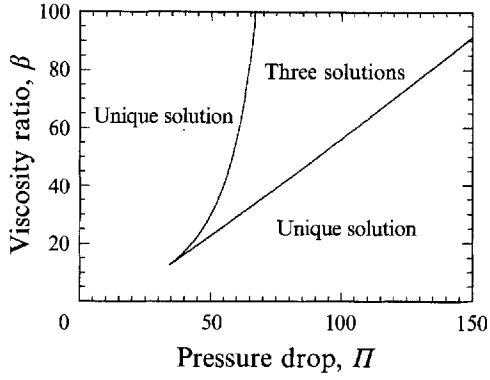

FIGURE 4. The (Π, β) plane is divided into regions where there is a unique solution and regions where there are three distinct solutions.

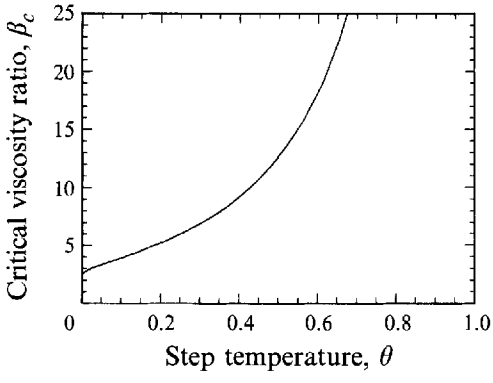

FIGURE 5. The critical viscosity ratio for the step-function viscosity model as a function of the temperature at which the step occurs.

average viscosity in the channel decreases sufficiently rapidly with increasing flow rate. Hence, a more abrupt variation of viscosity with temperature will, in general, lead to a lower value of the critical viscosity ratio. For example, the critical viscosity ratio for the exponential model is approximately 190, whereas the critical value for the step-function model with $\theta = 1/2$ is approximately 12.

For the step-function viscosity model, the temperature θ at which the change in viscosity occurs also has an effect on the critical viscosity ratio. As shown in figure 5, the critical value decreases as θ approaches the temperature of the wall. This can be understood by dividing the channel in the along-channel direction into three qualitative regions: an input region where the viscosity is $\mu(T_h)$ everywhere except for the thin boundary layers near the wall; a viscous region where the viscosity is $\mu(T_c)$ everywhere since the temperature has fallen below $T = \theta$ across the whole channel; and a changeover region in which the cross-channel average of the viscosity is significantly different from both initial and final values of the viscosity. Clearly, as θ decreases, the ratio of the length of the input region to that of the changeover region increases. Thus the lower the value of θ the more abrupt the viscosity change appears, which leads to a lower value of the critical viscosity ratio.

As $\theta \to 0$ the ratio of the input length to the changeover length is $O(|\ln\theta|)$. With a suitable choice of lengthscale, the cross-channel averaged viscosity in this limit

takes the value 1 in the input region $z < Q$ and β in the viscous region $z > Q$, and the changeover region can be neglected. This represents the most abrupt change in viscosity that is possible. A simple calculation shows that this will give a triple-valued solution if $\beta > 2$, which corresponds to the theoretical minimum value of β_c. This result is in agreement with the numerical results for $\theta \to 0$.

4. Linear stability of two-dimensional steady flows

We wish to investigate the linear stability of the basic two-dimensional steady states for different values of the parameters Π and β. Having obtained the basic state, which we now denote by a subscript zero, we introduce perturbations by writing

$$\boldsymbol{u}(y,z) = \boldsymbol{u}_0(y,z) + \mathbf{u}'(y,z)\mathrm{e}^{\sigma t+\mathrm{i}kx}, \tag{4.1a}$$

$$v(y,z) = v_0(y,z) + v'(y,z)\mathrm{e}^{\sigma t+\mathrm{i}kx}, \tag{4.1b}$$

$$T(y,z) = T_0(y,z) + T'(y,z)\mathrm{e}^{\sigma t+\mathrm{i}kx}, \tag{4.1c}$$

$$p(z) = p_0(z) + p'(z)\mathrm{e}^{\sigma t+\mathrm{i}kx}, \tag{4.1d}$$

where σ is the growth rate of the disturbance and k is the wavenumber of the disturbance in the x-direction. Since p' is independent of y and is thus symmetric in y, only symmetric perturbations to the velocity and temperature fields are coupled to p'. We expect the dynamical feedback giving rise to an instability to involve the pressure field via the effect of temperature on flow resistance and thus we concentrate on symmetric eigenmodes.

The linear stability problem then takes the form

$$\mu(T_0)w'_y + w_{0y}\left.\frac{\mathrm{d}\mu}{\mathrm{d}T}\right|_{T_0} T' = yp'_z, \tag{4.2a}$$

$$\mu(T_0)u'_y + u_{0y}\left.\frac{\mathrm{d}\mu}{\mathrm{d}T}\right|_{T_0} T' = \mathrm{i}kyp', \tag{4.2b}$$

$$\mathrm{i}ku' + v'_y + w'_z = 0, \tag{4.2c}$$

$$\sigma T' + v'T_{0y} + w'T_{0z} + v_0T'_y + w_0T'_z = T'_{yy}\,. \tag{4.2d}$$

The appropriate symmetric boundary conditions are

$$T' = 0 \text{ and } u' = v' = w' = 0 \text{ at } y = 1, \tag{4.2e}$$

$$T'_y = 0 \text{ and } v' = 0 \text{ at } y = 0, \tag{4.2f}$$

$$p' = 0 \text{ and } T' = 0 \text{ at } z = 0, \tag{4.2g}$$

$$p' = 0 \text{ at } z = 1. \tag{4.2h}$$

When the step-function viscosity model is employed the approach is, once again, slightly modified. In addition to (4.1), we perturb the position of the isotherm $T = \theta$ by writing

$$Y(z) = Y_0(z) + Y'(z)\mathrm{e}^{\sigma t+\mathrm{i}kx} \tag{4.1e}$$

and again linearize to obtain the same system as (4.2) but with the terms involving $\mathrm{d}\mu/\mathrm{d}T$ omitted. The conditions to be applied across the interface are

$$[\boldsymbol{u}'] + Y'[\boldsymbol{u}_{0y}] = 0 \qquad [v'] + Y'[v_{0y}] = 0 \qquad [\mu u'_y] = 0 \tag{4.3a,b,c}$$

$$[T'_y] = 0, \qquad [T'] = 0, \tag{4.3d,e}$$

$$Y'(x) = \frac{T'(x, Y_0(x))}{T_{0y}(x, Y_0(x))}, \tag{4.3f}$$

where square brackets denote the jump in the enclosed quantity across the isotherm $T = \theta$.

If we consider modes that are two-dimensional and neutrally stable (i.e. $k = 0$ and $\sigma = 0$) then the eigenfunctions take a particularly simple form. In this case the disturbance equations and the two-dimensional basic-state equations have essentially the same form and so the eigenfunctions for the linear stability problem result from an infinitesimal change in the input flow rate. We thus need a two-dimensional steady state which possesses the property that an infinitesimal increase in flow rate leaves the pressure drop unchanged. It follows that the states that are neutrally stable to two-dimensional perturbations correspond exactly with states at the local maximum and minimum of the curve relating pressure drop and flow rate. Physical considerations suggest that the central branch of this curve, in which the pressure drop decreases with increasing flow rate, corresponds to flows that are unstable to two-dimensional perturbations, while the slow and fast branches correspond to flows that are stable to two-dimensional perturbations.

4.1. *Numerical scheme*

We wish to solve the eigenvalue problem (4.2) for a range of values of Π. The standard method for solving such a system would be to seek $\sigma(\Pi, k)$ by first fixing Π and k and then solving for σ using finite-difference, finite-element or shooting methods. The process would then be repeated for each value of Π and k. Both finite-difference and finite-element methods would require inversion of very large matrices, and shooting, although clearly possible, requires the solution of a nonlinear complex equation.

Exploratory application of a shooting method suggested that there is one real eigenvalue with the rest of the spectrum made up of complex eigenvalues, and that the real eigenvalue always represents the most dangerous mode. Since the required eigenvalue is real, an alternative and much more efficient numerical method is possible.

Recall that the efficiency of the method used to determine the two-dimensional steady state was essentially due to the fact that the single downstream boundary condition at $z = 1$ could be satisfied by rescaling a solution that satisfied $p_z = -1$ at $z = 0$. With similar motivation, rather than solving for $\sigma(\Pi, k)$ we solve for $\Pi(\sigma, k)$ by fixing σ and k and considering the system (4.2) with the boundary condition $p' = 0$ at $z = 1$ replaced by $p'_z = -1$ at $z = 0$. As in §3 we denote the variables in this system with tildes. We then integrate numerically until $\tilde{p}' = 0$ at some value of $\tilde{z}$, say $\tilde{z}_1$. Then σ is an eigenvalue for the system when $Q = 2/3\tilde{z}_1$. This process must be repeated for a range of σ values, but nonlinear equation solving and large matrix operations have been avoided. The method for along-channel integration was similar to the method used to obtain the basic state and again takes into account the self-similar nature of the solution close to the channel entrance.

4.2. *Results*

We use the step-function viscosity model and begin by considering the stability to two-dimensional disturbances ($k = 0$). It is found that when $\beta < \beta_c$ and there is only one steady state, then it is stable. When $\beta > \beta_c$ and there are three steady states then, as predicted above, the slow and fast branches are stable and the central branch is unstable with the change of stability located at the local maximum and minimum.

We now turn our attention to the effect of three-dimensional disturbances ($k \neq 0$). Since the basic states cannot be uniquely determined by the value of Π when $\beta > \beta_c$, we label the basic state by the flow rate Q. While this now gives a unique identification

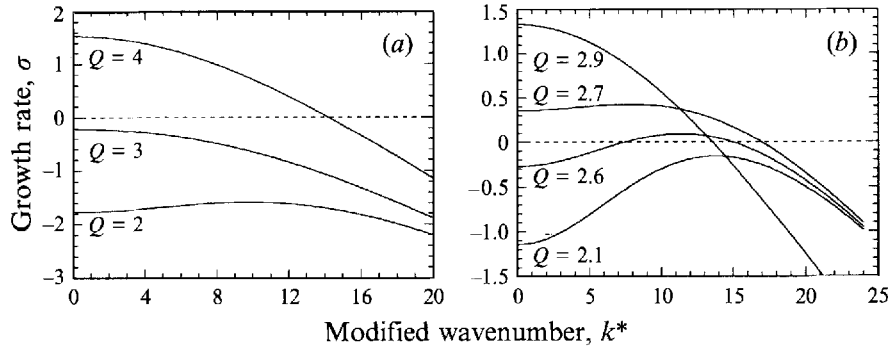

FIGURE 6. The dispersion relationship $\sigma(k^*)$ for various values of the flow rate: (*a*) viscosity ratio $\beta = 20$, which is between β_c and β_{3d}; (*b*) $\beta = 30$ which is greater than β_{3d}. The step-function viscosity model is used with the step at $\theta = 1/2$.

of the basic state, it should be stressed that the boundary conditions are those of fixed pressure drop and not those of fixed flow rate.

We expect that interesting phenomena will occur when the wavelength of the disturbance is comparable to the thermal entry length. With this in mind we introduce a modified wavenumber

$$k^* = k/Q, \tag{4.4}$$

which is scaled on a thermal entry lengthscale $O(wd^2/\kappa)$ rather than the length of the channel. We note that $wd^2/\kappa \gg d$ so that diffusion of temperature in the (x, z)-plane remains negligible.

For different values of Q and β the dispersion relation, $\sigma \equiv \sigma(k^*)$, can be characterized as being in one of two distinct regimes. Firstly, for sufficiently high flow rates the growth rate decreases monotonically with increasing k^* (figure 6*a*). Hence the value of k^* for which the largest growth rate occurs, which we define as $k^*_{max}(Q, \beta)$, is zero. This implies that in this parameter range the most unstable or the least stable mode is the one associated with two-dimensional disturbances. Secondly, at the lower flow rates the growth rate increases with k^* until it reaches a maximum at $k^*_{max}(Q, \beta) \neq 0$ and beyond that point decreases monotonically (figure 6*b*). We denote the boundary separating these two regimes by $Q_{3d}(\beta)$. If we examine the behaviour close to the boundary we see that the transition is continuous in the sense that the three-dimensional disturbances develop continuously from the two-dimensional disturbances, since if we start in the second regime and move toward the boundary the value of $k^*_{max}(Q, \beta)$ tends uniformly to zero.

When considering three-dimensional stability, a steady state is linearly stable if it is stable to disturbances of all wavenumbers. For values of β below and slightly above β_c the addition of three-dimensional modes does not affect the bifurcation structure since a solution that is stable to two-dimensional disturbances is also stable to all three-dimensional disturbances. A change occurs when the curve $Q = Q_{3d}(\beta)$ crosses the two-dimensional neutral-stability curve at a value of β which we denote by β_{3d}. When $\beta > \beta_{3d}$ there are now basic states which are stable to two-dimensional disturbances but are unstable to a finite band of wavenumbers with $k^* \neq 0$. This extends the region of instability from the two-dimensional result, modifying the neutral-stability boundary as seen in figure 7. Contours of the growth rate in (k^*, Q)-space are shown in figure 8 for $\beta < \beta_{3d}$ and $\beta > \beta_{3d}$.

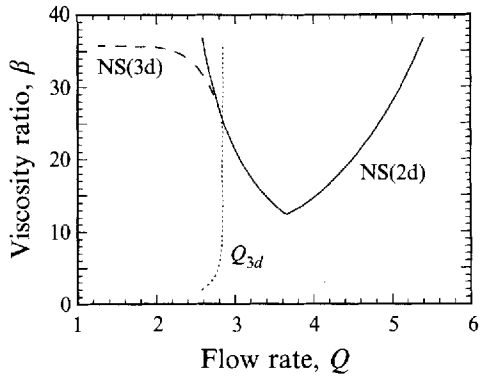

FIGURE 7. The inclusion of three-dimensional perturbations modifies the neutral-stability curve from the two-dimensional results. The solid curve NS(2d) is the two-dimensional neutral-stability boundary. The dotted curve Q_{3d} bounds the region where some three-dimensional disturbances have larger growth rates than two-dimensional disturbances. The dashed curve NS(3d) is the modification to the neutral-stability boundary when three-dimensional disturbances are taken into account. The step-function viscosity model is used with the step at $\theta = 1/2$.

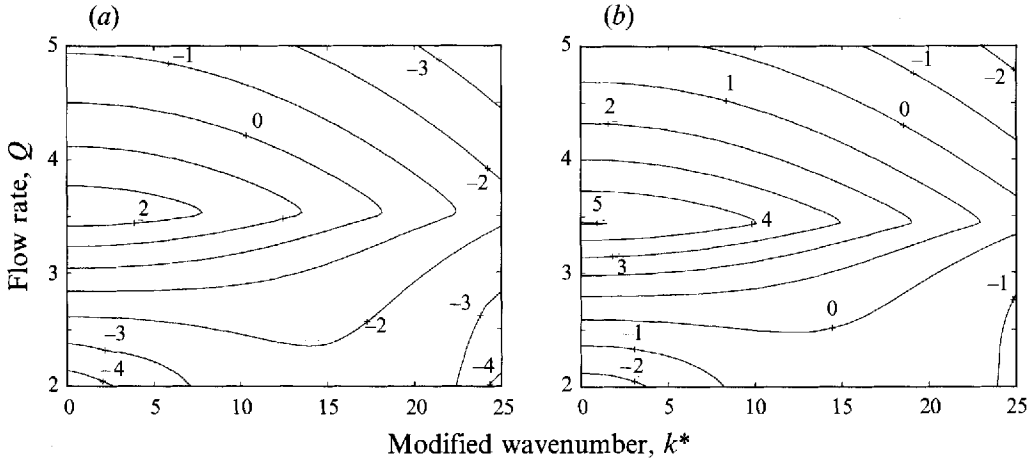

FIGURE 8. Contours of growth rate, σ, in (Q, k^*)-space are shown for $\beta = 20 < \beta_{3d}$ in (a) and for $\beta = 30 > \beta_{3d}$ in (b). The zero contour separates the unstable and stable regions.

As Q tends to zero the value of k^*_{max} tends to a finite value. In this limit the majority of the cooling occurs near the entrance of the channel while the remainder of the channel contains cold isoviscous fluid at temperature $T < \theta$. Hence, as expected, for slow flow rates the wavenumber of the most unstable or least stable mode is determined by the lengthscale over which the cooling occurs rather than the whole length of the channel.

Some physical understanding of these results can be provided by comparison with the Saffman–Taylor (1958) instability, in which the interface separating two fluids of different viscosities is unstable if the fluid of lower viscosity flows toward the fluid of higher viscosity. Returning to the present problem, when the flow is sufficiently slow the fluid will lose most of its heat by the time it reaches the exit and so have a viscosity close to $\mu(T_c)$. This gives rise to strong viscosity gradients in the along-channel direction, and so fluid of low viscosity is flowing into fluid of high viscosity. Thus, by analogy with the Saffman–Taylor instability, we might expect three-dimensional effects to emerge. However, when the flow is sufficiently rapid

the regions of high viscosity are found only in thin boundary layers adjacent to the walls and so viscosity gradients in the along-channel direction should in general be small, thus giving no reason to expect three-dimensional effects to emerge. These considerations provide us with some physical explanation of why the slow flow regimes are affected by three-dimensional modes whereas the fast flow regimes are not.

Although there are obvious similarities between the present problem and the Saffman–Taylor problem there are also significant differences. Firstly, for the case of continuous viscosity variation the current problem has no interface, though there is still a transition from low to high viscosity. Secondly, and more importantly, the variation in viscosity is not fixed to fluid elements and simply advected, since the viscosity of each element also evolves owing to the diffusion of heat. As a result, the stability domain and dispersion relationship differ from those associated with the Saffman–Taylor instability.

5. Three-dimensional steady flows

In this section we prove a surprising result which greatly simplifies the three-dimensional steady-state equations by establishing a strong correspondence between three-dimensional and two-dimensional steady states. The result holds irrespective of the particular geometry of the boundaries in the (x, z)-plane.

We begin by using the lubrication equation (2.5*a*) along with the boundary conditions $\boldsymbol{u} = \boldsymbol{0}$ on $y = 1$ and $\boldsymbol{u}_y = \boldsymbol{0}$ on $y = 0$, to write $\boldsymbol{u}$ in the form

$$\boldsymbol{u} = -\mathscr{U}(y; T)\nabla p, \tag{5.1}$$

where $\mathscr{U}(y; T)$ is a function of y and a functional of T defined by

$$\mathscr{U} = \int_y^1 \frac{\check{y}\,\mathrm{d}\check{y}}{\mu(T(x, \check{y}, z))}. \tag{5.2}$$

Substitution of this into the equation of local incompressibility (2.6) along with the boundary condition $v = 0$ on $y = 1$ yields

$$v = -(\nabla^2 p + \nabla p \cdot \nabla) \int_y^1 \mathscr{U}\,\mathrm{d}y. \tag{5.3}$$

We define the local, cross-channel-averaged volume flux by

$$\boldsymbol{q} = 2\int_0^1 \boldsymbol{u}\,\mathrm{d}y, \tag{5.4}$$

which, by using (5.1), can be expressed in the form

$$\boldsymbol{q} = -\mathscr{Q}(T)\nabla p, \tag{5.5}$$

where $\mathscr{Q}$ is a functional of T defined by

$$\mathscr{Q}(T) \equiv 2\int_0^1 \int_y^1 \frac{\check{y}\,\mathrm{d}\check{y}}{\mu(T(x, \check{y}, z))}\,\mathrm{d}y. \tag{5.6}$$

Hence the equation of global continuity,

$$\nabla \cdot \boldsymbol{q} = 0, \tag{5.7}$$

which follows by integration of (2.6) across the channel, can be written as

$$(\nabla^2 p + \nabla p \cdot \nabla)\mathscr{Q} = 0. \tag{5.8}$$

Using (5.5) and (5.8) to eliminate p from (5.3), we obtain

$$v = \boldsymbol{q} \cdot \nabla \left(\frac{1}{\mathscr{Q}} \int_y^1 \mathscr{U} \, \mathrm{d}y \right). \tag{5.9}$$

Thus the steady temperature equation,

$$\boldsymbol{u} \cdot \nabla T + v T_y = T_{yy}, \tag{5.10}$$

can be expressed in the form

$$\frac{\mathscr{U}}{\mathscr{Q}} \boldsymbol{q} \cdot \nabla T + \boldsymbol{q} \cdot \nabla \left(\frac{1}{\mathscr{Q}} \int_y^1 \mathscr{U} \, \mathrm{d}y \right) T_y = T_{yy}. \tag{5.11}$$

Since $\mathscr{U}$ and $\mathscr{Q}$ depend only on the cross-channel temperature profile at a given x and z, the only explicit dependence on x and z in (5.11) occurs in the operator $\boldsymbol{q} \cdot \nabla$, which describes variation along the streamlines of the two-dimensional averaged flow field $\boldsymbol{q}(x, z)$. We rescale the variation along these streamlines by introducing a time-like variable $\tau(x, z)$ that satisfies

$$\boldsymbol{q} \cdot \nabla \tau = 1 \tag{5.12}$$

subject to $\tau = 0$ at the entrance to the channel. Thus (5.11) becomes

$$\frac{\mathscr{U}}{\mathscr{Q}} \frac{\partial T}{\partial \tau} + \frac{\partial}{\partial \tau} \left(\frac{1}{\mathscr{Q}} \int_y^1 \mathscr{U} \, \mathrm{d}y \right) T_y = T_{yy}, \tag{5.13}$$

where $\partial / \partial \tau$ is the derivative following a fixed streamline of $\boldsymbol{q}$. The variable τ can be interpreted physically as an averaged measure of the time taken for fluid to reach a given x and z, though it should be remembered that the fluid by the walls is stationary and that on the centreline is moving faster than $\boldsymbol{q}$.

Equation (5.13) takes the same form as the two-dimensional steady-state temperature equation with unit input flow rate and z replaced by τ. Hence we deduce the surprising result that along the streamlines of the average flow field $\boldsymbol{q}$ the cross-channel temperature profile maintains the same form as in the two-dimensional steady state. The result depends on the fact that, by using global continuity, both $\boldsymbol{u}$ and v can be expressed solely in terms of ∇p, or $\boldsymbol{q}$, and the cross-channel temperature profile. In particular, the key step seems to be the elimination of $\nabla^2 p$, which is influenced by neighbouring streamlines, from (5.3) using (5.8). (We note the generalization that a steady temperature field in a channel of non-uniform width $2h(x, z)$ can be obtained from the two-dimensional steady state in a uniform channel by modifying the definition of τ in (5.12) to $\boldsymbol{q} \cdot \nabla \tau = h$, where $\boldsymbol{q} = -h^3 \mathscr{Q} \nabla p$, and stretching the temperature profile at each τ by a factor h.)

Having established this correspondence between the temperature distribution in a general three-dimensional steady state and that in two-dimensional steady flow with $\boldsymbol{q} = (0, 0, 1)$, we define an average viscosity $\bar{\mu}(\tau)$ by

$$\bar{\mu}(\tau) \equiv \left[\mathscr{Q}\Big(T(y, \tau) \Big) \right]^{-1}, \tag{5.14}$$

where $T(y, \tau)$ is the solution of (5.13). Hence the three-dimensional steady-state equations can be written as

$$\nabla \cdot \boldsymbol{q} = 0, \qquad \boldsymbol{q} \cdot \nabla \tau = 1, \qquad \bar{\mu}(\tau) \boldsymbol{q} = -\nabla p. \tag{5.15}$$

The boundary conditions are $\tau = 0$ at the entrance of the channel together with conditions on the pressure which will depend upon the particular geometry in question. The advantage of this formulation is that all the cross-channel structure is embodied in the known function $\bar{\mu}$, thus reducing the problem from three dimensions to the two-dimensional (x, z)-plane.

A number of previous studies (Whitehead & Helfrich 1991; Bercovici 1992, 1994; Helfrich 1995) of temperature-dependent lubrication flows have used *ad hoc* cross-channel averages based on parabolic velocity and temperature profiles, which result in equations similar to (5.15). When the fluid has travelled a distance much greater than the thermal entry length such an averaged approach is clearly valid. However, in the region in which interesting dynamical behaviour or instability is predicted by these models the distance travelled by the fluid is comparable to the thermal entry length and thus the assumption that the flow can be well represented by cross-channel-averages appears at first sight to be invalid. However, the above result shows that, provided suitable weighted averages are taken and an appropriate average viscosity model $\bar{\mu}$ is chosen, the approach is certainly a valid way to determine steady states. It should be noted, however, that the non-steady behaviour of a cross-channel averaged model need not be the same as that of the full model.

Without detailed calculation of $\bar{\mu}$ from the full solution of (5.13) for a given $\mu(T)$, an appropriate empirical choice for the functional form of $\bar{\mu}$ is a non-trivial matter. Evidently, the function $\bar{\mu}(\tau)$ must be monotonic with $\bar{\mu}(0) = 1$ and $\bar{\mu}(\infty) = \beta$. As shown in Appendix B it is possible to derive conditions on $\bar{\mu}$ such that the solution to (5.15) exhibits both a non-monotonic relationship between pressure drop and flow rate and the property that the slow branch becomes destabilized by the effect of three-dimensional disturbances. However, a simple functional form for $\bar{\mu}$ may not always yield all of the required properties. For example, Whitehead & Helfrich (1991) adopted a form in which the averaged viscosity was unity upstream of one thermal entry length and β downstream of one thermal entry length. This form for $\bar{\mu}$ produces the non-monotonic flow rate curve, but a simple calculation shows that the slow branch is not destabilized in this case and hence three-dimensional disturbances are never the most rapidly growing modes.

6. Three-dimensional flow-focused steady states

When the slow branch of the curve relating pressure drop and flow rate becomes unstable to three-dimensional disturbances a slight increase in the viscosity near some value of x will lead to a decrease in the along-channel velocity which will decrease the advected heat supply and thus cause the fluid to become more viscous. A slight decrease in the viscosity at a neighbouring value of x will have the opposite effect. The difference in pressure between these values of x cause transverse flows which accentuate this mechanism and lead to even stronger transverse flows. It seems plausible that this mechanism will eventually cease and that the growth of the disturbance might be saturated by the formation of a three-dimensional steady state.

Unfortunately, when calculating three-dimensional flows we are unable to make a coordinate rescaling analogous to that described in §3 for the solution of the two-dimensional equations and so we must employ an alternative technique to obtain the solution. Rather than attempt the computationally intensive solution of the time evolution of the full three-dimensional equations towards a steady state, we make use of the result derived in §5 and work with the cross-channel-averaged model. In order to construct an iterative numerical method, we replace the operator $\boldsymbol{q} \cdot \nabla$ in

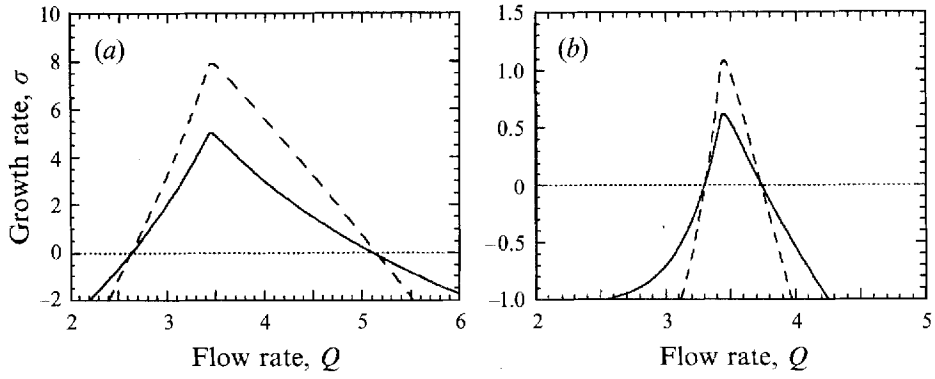

FIGURE 9. Growth rates for both the full system (solid line) and the cross-channel-averaged system (dashed line) for $\beta = 30$. (*a*) $k^* = 0$, (*b*) $k^* = 25$. The points of neutral stability in the two systems coincide.

(5.15) by $\partial_{\bar{t}} + \boldsymbol{q} \cdot \nabla$, where $\bar{t}$ is a pseudo-time, corresponding to the iteration parameter. Elimination of $\boldsymbol{q}$ then yields

$$\frac{\partial \tau}{\partial \bar{t}} - \frac{\nabla p \cdot \nabla \tau}{\bar{\mu}(\tau)} = 1, \tag{6.1a}$$

$$\nabla \cdot \left(\frac{\nabla p}{\bar{\mu}(\tau)} \right) = 0. \tag{6.1b}$$

with boundary conditions

$$p = 0 \quad \text{and} \quad \tau = 0 \quad \text{at} \quad z = 0, \tag{6.1c}$$

$$p = -\Pi \quad \text{at} \quad z = 1. \tag{6.1d}$$

We also choose a finite rectangular domain and adopt periodic boundary conditions in x, which essentially fixes the wavenumber in the x-direction of any three-dimensional state.

The unique correspondence shown in §5 between steady states in the full three-dimensional system and in the cross-channel-averaged system suggests that the stability boundaries in the two systems will be identical if the bifurcation to instability involves a three-dimensional steady state. Hence the stability of steady states in the full three-dimensional system should be the same as the pseudo-time stability of the cross-channel-averaged system. This is illustrated in figure 9 where the growth rates (in real time and pseudo-time) are shown for a given basic state. The stability is indeed seen to agree and other calculations found no differences between the stability boundaries of the two systems. However, the growth rates are different, with the exception of states which have neutral growth rate, thus illustrating the point that the unsteady evolution of the systems may be different.

The pseudo-time evolution of (6.1) is not, in itself, of interest with regard to the full system, since our purpose is to iterate to a steady state. Hence we are justified in the use of a low-order method for pseudo-time stepping. We adopt a finite-difference approach and solve (6.1*a*) by first-order explicit time-stepping, with the time-step constrained by a Courant condition, while the spatial derivatives are evaluated by an upwinding technique. This gives the new distribution of τ. Since the pressure distribution changes slowly from one pseudo-time step to the next the elliptic problem (6.1*b*) is best solved by an iterative rather than a direct method.

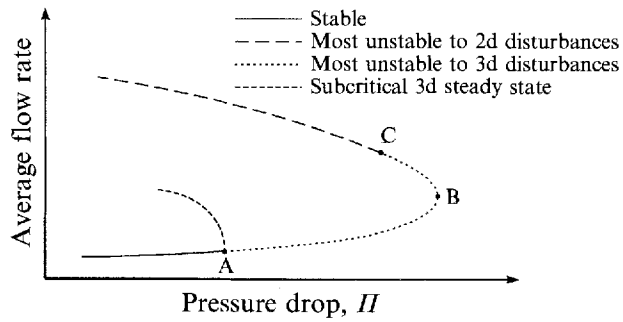

FIGURE 10. Schematic of the local bifurcation structure near the point where the slow branch of the curve relating pressure drop to flow rate becomes unstable to three-dimensional disturbances. The points A, B, C correspond to the intersection of $\beta = \text{const}$ with the curves NS(3d), NS(2d) and Q_{3d} in figure 7.

Thus we adopt an Alternating Direction Implicit (ADI) method with second-order finite-differences in both the x- and z-directions to find the new value of the pressure distribution. We then make the next explicit time step to calculate the distribution of τ and continue in the obvious way until a steady state is achieved. The spatial accuracy of this method was checked by comparison of the results of the two-dimensional calculation (§3) with steady solutions of (6.1) in which there is no x variation in the solution.

As discussed above, the stability of unidirectional solutions of the cross-channel-averaged model (6.1) is the same as that of the full model (figure 7). The obvious place to seek three-dimensional (flow-focused) steady states is near where the slow branch becomes unstable to three-dimensional disturbances. However, despite using a continuation method based on a slow variation of parameters from a stable solution, we were unable to find any three-dimensional steady states beyond the bifurcation point. Instead, all unstable solutions continued to evolve with pseudo-time. There are indications that unstable flows always evolve in the averaged model onto the fast branch, though this has yet to be confirmed. It should also be noted again that the pseudo-time evolution of the averaged model may not be analogous to the evolution of the full model. However, the non-existence of supercritical steady states near the bifurcation on the slow branch in the cross-channel-averaged system does imply the non-existence of similar supercritical steady states in the full system. The calculation in §4 shows that the slow branch becomes unstable to three-dimensional disturbances via a stationary bifurcation and so we conclude that there must be a subcritical pitchfork bifurcation at this point (figure 10) (e.g. Guckenheimer & Holmes 1983, section 3.4).

7. Discussion

We have analysed planar channel flow in which large viscosity changes occur owing to cooling from the sidewalls. A variety of phenomena has been demonstrated, including a nonlinear and possibly non-monotonic relationship between the pressure drop and the flow rate and linear instability to two-dimensional or three-dimensional disturbances.

For sufficiently large viscosity contrasts and certain values of the fixed pressure drop there are three possible two-dimensional steady states corresponding to different

flow rates. In real geological situations the pressure in the magma chamber which drives the flow will decrease with time. If this decrease occurs sufficiently slowly then the present analysis will give the relationship between the pressure drop at a given time and the flow rate at that time. Suppose that the variation in viscosity of the magma is sufficiently large to allow triple solutions and the initial pressure in the chamber is sufficiently large that the initial flow is on the fast branch. Then, as the pressure in the chamber gradually decreases, the flow rate will also gradually decrease until the pressure drop falls below the point where the fast branch ends. At this point the flow rate will undergo a hysteretic jump taking it onto the slow branch. It follows that a rapid decrease in the eruption rate may correspond to a change of solution branch rather than to a sudden decrease in the magma chamber pressure.

When three two-dimensional steady states exist it has been shown that the central branch is always unstable, as one might expect from physical arguments, with the fast and slow branches always stable to two-dimensional disturbances. It has also been shown that, when three-dimensional disturbances are considered, part of the slow branch can become unstable. The mechanism which makes the modes associated with three-dimensional disturbances more unstable or less stable than the modes associated with two-dimensional disturbances can be understood physically by analogy with the Saffman–Taylor (1958) instability. There are however a number of important differences. In the Saffman–Taylor instability the interface between the regions of different viscosity is fixed to fluid elements, whereas in the current problem the location of the viscosity variation is determined by the temperature in the fluid. Also the effect of three-dimensional disturbances on the growth rate is superimposed onto a steady state which has, in general, a non-zero growth rate for two-dimensional disturbances.

Bruce & Huppert (1990) argued that three-dimensional instabilities would arise even for large flow rates when the temperature variation is confined to thin boundary layers adjacent to the wall. We find that this is not the case and that states on the fast branch are always stable to three-dimensional disturbances. However, the analysis does show that their physical arguments suggesting three-dimensionality of solutions are valid for lower flow rates. There are however important differences between the flow analysed in the current work and that analysed by Bruce & Huppert. Their solution is implicitly time dependent which precludes a formal stability analysis. Another difference is that in both problems the flow resistance depends on the temperature of the fluid, but the dependency in Bruce & Huppert's analysis was due to an increase or decrease in the width of the channel by melting or solidification rather than to variation in viscosity.

Motivated by the fact that the two-dimensional steady states are unstable under certain conditions, we used the result obtained in §5 to facilitate the search for three-dimensional steady states. The result showed that, by taking appropriate cross-channel averages the three-dimensional steady-state equations are equivalent to a two-dimensional system together with a suitably averaged viscosity function, which must be calculated by integrating the full system with unit input flow rate. This result provides some support for the averaged systems which have been used in a number of previous studies (Whitehead & Helfrich 1991; Bercovici 1992, 1994; Helfrich 1995), though it should be noted both that the true unsteady behaviour may not be imitated by the averaged system and that care is necessary to choose a suitable averaged viscosity.

An interesting extension of this work would be an exploration of the bifurcation structure of the whole parameter space. Also, an experiment could confirm the

findings of the analysis. This could be most conveniently carried out using a fluid that exhibits large viscosity contrasts around room temperature such as glycerol, which increases in viscosity by a factor of about 1000 between 0°C and 100°C and shows even steeper increases when cooled below 0°C. We close by noting that thermo-viscous coupling is an interesting general area with a number of problems still to be analysed.

Appendix A. The basic flow for a step-function viscosity model

In §3 we derived the equations governing the mass and heat transport for a continuous dependence of viscosity on temperature. In this Appendix we summarize the solutions for the velocity profile when the step-function model (2.9*b*) is used.

The viscosity is piecewise constant and so the along-channel component of velocity is composed of parabolic segments. The segments depend on the position of the isotherm $T = \theta$, which we denote $Y(z)$, and are given by

$$w = \begin{cases} \dfrac{p_z}{2\beta}\left(y^2 - 1\right) & \text{in } Y(z) < y < 1 \\ \dfrac{p_z}{2\beta}\left(\beta y^2 - (\beta - 1)Y^2 - 1\right) & \text{in } 0 < y < Y(z), \end{cases} \tag{A 1a}$$

where the pressure gradient is given by

$$p_z = \frac{-\beta}{1 + (\beta - 1)Y^3}, \tag{A 1b}$$

and the cross-channel components of velocity are given by integration of (2.6).

The near-entrance similarity solution also takes a slightly different form to the case of continuous viscosity variation (3.5) and can be solved explicitly. We introduce similarity variables

$$\eta = \frac{(1 - y)}{z^{1/3}}, \qquad c = \frac{1 - Y}{z^{1/3}}, \tag{A2a,b}$$

$$T = \begin{cases} g_1(\eta) & \text{for } Y(z) < y < 1 \\ g_2(\eta) & \text{for } 0 < y < Y(z), \end{cases} \tag{A2c}$$

and, after substitution into (2.4), (2.7*a*) and (2.7*c*) and retention of only the leading-order terms in z, we obtain

$$3\beta \frac{\mathrm{d}^2 g_1}{\mathrm{d}\eta^2} + \eta^2 \frac{\mathrm{d}g_1}{\mathrm{d}\eta} = 0, \qquad 3\beta \frac{\mathrm{d}^2 g_2}{\mathrm{d}\eta^2} + \left((\beta - 1)(\eta - c)^2 + \eta^2\right) \frac{\mathrm{d}g_2}{\mathrm{d}\eta} = 0, \tag{A3a}$$

subject to boundary conditions

$$g_1(0) = 0, \qquad g_1(c) = g_2(c) = \theta, \qquad \frac{\mathrm{d}g_1}{\mathrm{d}\eta}(c) = \frac{\mathrm{d}g_2}{\mathrm{d}\eta}(c), \qquad g_2(\infty) = 1. \tag{A3b}$$

This system can readily be solved to yield the condition

$$\int_c^\infty \exp\left[-\{(\beta - 1)(\eta - c)^3 + \eta^3\}/9\beta\right] \mathrm{d}\eta = \frac{(1 - \theta)}{\theta} \int_0^c \exp\left[-\eta^3/9\beta\right] \mathrm{d}\eta, \tag{A4}$$

which must be solved numerically for c.

Appendix B. The neutral stability curve for the averaged model (5.17)

In §4 we showed that the region of instability to two-dimensional disturbances for the full model (2.4)–(2.7) corresponds to the region between the turning points on the curve of pressure drop versus flow rate when $\beta > \beta_c$. For $\beta_c < \beta < \beta_{3d}$ the inclusion of three-dimensional disturbances does not extend the region of instability, but for $\beta > \beta_{3d}$ the region of instability is extended to include slow flows that are stable to two-dimensional disturbances. In this Appendix we derive conditions for similar results to hold in the averaged model (5.15)

As in §3 we rescale the coordinates so that

$$\boldsymbol{q} = (0,0,1) \text{ on } z = 0 \qquad \text{and} \qquad p = -4\Pi^2/9Q^2 \text{ on } z = 2/3Q.$$

The basic steady solution of (5.15) is then

$$\boldsymbol{q} = (0,0,1), \qquad \tau = z, \qquad p = -\mathscr{I}[\bar{\mu}], \tag{B1a,b,c}$$

where

$$\mathscr{I}[f] \equiv \int_0^z f(\check{z})\mathrm{d}\check{z}.$$

We seek neutrally stable linear eigenmodes and let

$$\boldsymbol{q} = (0,0,1) + \epsilon(\bar{u}'(z),0,\bar{w}'(z))\mathrm{e}^{\mathrm{i}kx} \tag{B2a}$$

$$\tau = z + \epsilon\tau'(z)\mathrm{e}^{\mathrm{i}kx}, \quad p = -\mathscr{I}[\bar{\mu}] + \epsilon p'(z)\mathrm{e}^{\mathrm{i}kx}. \tag{B2b,c}$$

Substitution of (B2) into (5.15) followed by linearization yields

$$\bar{\mu}(z)\bar{w}' + \bar{\mu}_z(z)\tau' = p'_z, \quad \bar{\mu}(z)\bar{u}' = \mathrm{i}kp', \tag{B3a,b}$$

$$\bar{w}' + \tau'_z = 0\,\mathrm{i}k\bar{u}' + \bar{w}'_z = 0, \tag{B3c,d}$$

which must be solved subject to the boundary conditions

$$\tau'(0) = p'(0) = p'(2/3Q) = 0. \tag{B3e}$$

For a given value of k, we integrate (B3) to find the zeros of $p'(z)$ and thus obtain the values of Q which are neutrally stable for that wavenumber.

When $k = 0$ integration of (B3) yields

$$\boldsymbol{q}' = (0,0,1) \qquad \tau' = z \qquad p' = 2\mathscr{I}[\bar{\mu}] - z\bar{\mu}. \tag{B4a,b,c}$$

Thus the condition for neutrally stable two-dimensional modes, and hence for turning points on the curve of pressure drop versus flow rate, is that $\bar{\mu}$ gives $p' = 0$ in (B4c) for some $z = 2/3Q$. If $\bar{\mu}$ is monotonic then the first zero (z_{min}) will correspond to a local minimum on the pressure drop versus flow rate curve and the second zero (z_{max}) will correspond to a local maximum.

We now consider how the introduction of three-dimensional disturbances affects the neutral-stability boundary. We expand the linear eigenmode for $k \ll 1$ by

$$\bar{u}' = k\bar{u}'_1, \quad \bar{w}' = 1 + k^2\bar{w}'_1 \tag{B5a,b}$$

$$\tau' = \tau'_0 + k^2\tau'_1, \quad p' = p'_0 + k^2 p'_1, \tag{B5c,d}$$

where τ_0' and p_0' are given by (B4). Integration of the $O(k^2)$ terms in (B5) yields

$$p_1' = 2\mathscr{I}\left[\bar{\mu}\mathscr{I}\left[\frac{p_0'}{\bar{\mu}}\right]\right] - \bar{\mu}\mathscr{I}^2\left[\frac{p_0'}{\bar{\mu}}\right]. \tag{B6}$$

If we evaluate p_1' at the zero of (A5) that corresponds to the local maximum in the pressure drop versus flow rate curve we can infer whether the effect of small wavenumber is stabilizing or destabilizing. If $p_1' > 0$ then the effect of small k is to move the neutral mode into the region which is unstable to $k = 0$ and so in this case small k is stabilizing. However, if $p_1' < 0$ then the opposite is true and therefore the condition for destabilization of the slow branch is

$$p_1'(z_{max}) < 0, \tag{B7}$$

where p_1' and p_2' are related to $\bar{\mu}$ by (B4*c*) and (B6).

REFERENCES

BERCOVICI, D. 1992 Wave dynamics in mantle plume heads and hotspot swells. *Geophys. Res. Lett.* **19**, 1791–1794.

BERCOVICI, D. 1994 A theoretical model of cooling viscous gravity currents with temperature-dependent viscosity. *Geophys. Res. Lett.* **21**, 1177–1180.

BJÖRNSSON, A., JOHNSEN, G., SIGURDSSON, S., THORBERGSSON, G. & TRYGGVASON, E. 1979 Rifting of the plate boundary in North Iceland. *J. Geophys. Res.* **84**, 3029–3038.

BRUCE, P. M. & HUPPERT, H. E. 1990 Solidification and melting along dykes by the laminar flow of basaltic magma. In *Magma Transport and Storage* (ed. M. P. Ryan), pp. 87–101. John Wiley and Sons.

GUCKENHEIMER, J. & HOLMES, P. 1983 *Nonlinear Oscillations, Dynamical Systems, and Bifurcations of Vector Fields* Springer.

HELFRICH, K. R. 1995 Thermo-viscous fingering of flow in a thin gap: a model of magma flow in dikes and fissures. *J. Fluid Mech.* **305**, 219–238.

OCKENDON, H. & OCKENDON, J. R. 1977 Variable-viscosity flows in heated and cooled channels *J. Fluid Mech.* **83**, 177–190.

PRESS, W. H., TEUKOLSKY, S. A., VETTERLING, W. T. & FLANNERY, B. P. 1992 *Numerical Recipes in FORTRAN*, 2nd Edn, pp. 352–355. Cambridge University Press.

RICHARDSON, S. M. 1986 Injection moulding of thermoplastics: Freezing of variable-viscosity fluids. II. Developing flows with very low heat generation. *Rheol. Acta* **25**, 308–318.

RICHTER, D. H., EATON, J. P., MURATA, K. J., AULT, W. A. & KRIVOY, H. L. 1970 Chronological narrative of the 1959–60 eruptions of Kilauea volcano, Hawaii. *US Geol. Surv. Prof. Pap.* **537-E**, 1–73.

RYAN, M. P. & BLEVINS, J. Y. K. 1987 The viscosity of synthetic and natural silicate melts and glasses at high temperatures and 1 bar pressure and at high pressures. *US Geol. Survey. Bull.* **1764**, 1–563.

SAFFMAN, P. G. & TAYLOR, G. I. 1958 The penetration of a fluid into a porous medium or Hele-Shaw cell containing a more viscous liquid. *Proc. R. Soc. Lond.* A **245**, 312–329.

WHITEHEAD, J. A. & HELFRICH, K. R. 1991 Instability of flow with temperature-dependent viscosity: A model of magma dynamics. *J. Geophys. Res.* **96**, 4145–4155.